AGU PUBLICATIONS

Water Resources Research

RESEARCH ARTICLE
10.1002/2013WR014964

# High-resolution modeling of the spatial heterogeneity of soil moisture: Applications in network design

**Nathaniel W. Chaney[1], Joshua K. Roundy[1], Julio E. Herrera-Estrada[1], and Eric F. Wood[1]**

[1]Department of Civil and Environmental Engineering, Princeton University, Princeton, New Jersey, USA

**Key Points:**
- High-resolution modeling of soil moisture fields over the Little River Experimental Watershed
- Analysis of the main drivers of soil moisture heterogeneity
- Exploration of novel methods for network design

**Correspondence to:**
N. W. Chaney,
nchaney@princeton.edu

**Citation:**
Chaney, N. W., J. K. Roundy, J. E. Herrera-Estrada, and E. F. Wood (2015), High-resolution modeling of the spatial heterogeneity of soil moisture: Applications in network design, *Water Resour. Res.*, *51*, 619–638, doi:10.1002/2013WR014964.

Received 26 OCT 2013
Accepted 28 NOV 2014
Accepted article online 5 DEC 2014
Published online 28 JAN 2015

**Abstract** The spatial heterogeneity of soil moisture remains a persistent challenge in the design of in situ measurement networks, spatial downscaling of coarse estimates (e.g., satellite retrievals), and hydrologic modeling. To address this challenge, we analyze high-resolution (∼9 m) simulated soil moisture fields over the Little River Experimental Watershed (LREW) in Georgia, USA, to assess the role and interaction of the spatial heterogeneity controls of soil moisture. We calibrate and validate the TOPLATS distributed hydrologic model with high to moderate resolution land and meteorological data sets to provide daily soil moisture fields between 2004 and 2008. The results suggest that topography and soils are the main drivers of spatial heterogeneity over the LREW. We use this analysis to introduce a novel network design method that uses land data sets as proxies of the main drivers of local heterogeneity (topography, land cover, and soil properties) to define unique and representative hydrologic similar units (subsurface, surface, and vegetation) for probe placement. The calibration of the hydrologic model and network design method illustrates how the use of hydrologic similar units in hydrologic modeling could minimize computation and guide efforts toward improved macroscale land surface modeling.

## 1. Introduction

Soil moisture dynamics affects runoff generating processes, short-term weather prediction, soil erosion, solute transport, vegetation dynamics, drought processes, and evapotranspiration [*Crow et al*., 2012; *Famiglietti et al*., 1998; *Western et al*., 2004]. Its spatial heterogeneity plays an important role in evapotranspiration, runoff, precipitation, and atmospheric variability [*Famiglietti et al*., 2008; *Peters-Lidard et al*., 1997; *Quinn et al*., 1995]. This heterogeneity complicates the comparison of in situ observations to retrievals from airborne and satellite remote sensing [*Western et al*., 2004]. Although current and upcoming satellite missions (SMAP and SMOS) will provide retrievals at higher spatial resolutions, validation using fine-scale measurements and spatial downscaling will be necessary for the foreseeable future.

The drivers of soil moisture spatial heterogeneity include topography, vegetation, radiation, soil properties, meteorological forcing, and depth to water table [*Blöschl and Sivapalan*, 1995; *Famiglietti et al*., 1998; *Hawley et al*., 1983; *Mohanty et al*., 2000; *Rosenbaum et al*., 2012]. Although the literature agrees on the drivers, disagreement remains regarding the role and importance of each of these drivers as a function of climate, ecosystem, and areal averaged soil moisture [*Famiglietti et al*., 1998, 2008; *Rosenbaum et al*., 2012; *Vereecken et al*., 2007; *Western et al*., 2004; *Wilson et al*., 2005].

A strong relationship exists between the temporal evolution in the areal variance (proxy for spatial heterogeneity) and the areal mean [*Famiglietti et al*., 2008; *Western et al*., 1999]. The peak in areal variance occurs in the intermediate soil moisture ranges with the location of the peak varying between locations [*Rosenbaum et al*., 2012]. *Western et al*. [2004] relate these differences to the location's drivers of soil moisture heterogeneity including climate, topography, and soils. *Grayson et al*. [1997] show the existence of a rapid transition between two preferential states (wet and dry) due to a shift from nonlocal (lateral subsurface flow) to local (soil properties and evapotranspiration) drivers during the dry down period. Hysteresis observed in the soil moisture variability has been attributed to the complex interactions between the drivers of heterogeneity [*Rosenbaum et al*., 2012; *Vivoni et al*., 2010]. *Pan and Peters-Lidard* [2008] show the existence of a mean threshold value above which the variability increases during drying and below which the variability decreases due to evapotranspiration's homogenization of the field. This threshold value is the critical point where plants cease to transpire at the potential rate [*Rodriguez-Iturbe and Porporato*, 2004].

Due to soil moisture's low spatial correlation, in situ networks rarely provide sufficient coverage to capture the fine-scale spatial properties of soil moisture; as described in *Crow et al*. [2005], distributed land surface modeling may be a viable alternative. These models account for the interactions between the main components of the land surface (vegetation, surface, and subsurface) and directly account for distributed rainfall, vegetation, soil, and topography to simulate fine-scale soil moisture fields. The main reservations in adopting this approach are errors in the model assumptions, and physical parameterizations, and input data sets. These downfalls can partially be addressed through calibration of the model parameters using available in situ measurements.

The main goal of this study is to gain a more complete understanding of the controls of the seasonality of soil moisture heterogeneity over the Little River Experimental Watershed. This can lead to improved network design, spatial downscaling, and macroscale land surface modeling. We develop the high-resolution soil moisture fields (∼9 m) by driving the TOPLATS distributed land surface model using moderate to high-resolution meteorology, elevation, soil, and vegetation data sets over the Little River Experimental Watershed. The model is calibrated and validated using available in situ measurements. The analysis of the drivers of soil moisture heterogeneity is then used to inform the development of a novel technique for network design of ground measurements.

## 2. Data

### 2.1. Study Area

The Little River Experimental Watershed is a 334 $km^2$ catchment located in south-central Georgia, USA. It is representative of the climate, topography, soils, geology, stream networks, and agricultural production system in the Coastal Plain region [*Bosch et al*., 2007]. Broad, flat alluvial floodplains, river terraces, and gently sloping uplands characterize its low topographic relief with slopes ranging between flat and 12% [*Osmond et al*., 2012]. Streamflow originates due to a seasonally dependent shallow aquifer and surface runoff primarily in the low-lying, poorly drained, near-stream areas [*Bosch et al*., 2007; *Shirmohammadi et al*., 1986]. The catchment's soils, primarily sandy and loamy, are well drained and have fairly low water holding capacities. As of 2003, the watershed was 31% row crops and fallow agricultural land, 50% forest, 7% urban, 10% pasture, and 2% water [*Bosch et al*., 2007]. Crop production is predominant on moderately to well-drained upland soils and riparian forests and wetlands on poorly drained soils along streams [*Osmond et al*., 2012]. The region's climate is humid subtropical (∼1200 mm annual rainfall) with a long growing season. Rainfall is unevenly distributed throughout the year, with the greatest rainfall from January to March and June to August.

#### 2.1.1. Little River Experimental Watershed Network

The LREW measurement network has 7 stream gauges, 46 rain gauges, and 3 climate stations [*Bosch et al*., 2007]. The spacing between the precipitation gauges varies from 3 to 8 km. Seventeen of the rain gauge sites include Stevens-Vitel soil moisture sensors at 5, 20, and 30 cm [*Jackson et al*., 2006]. The measurements taken every 5 min are averaged and reported at a 30 min time step. We use all soil moisture and precipitation data available between 2004 and 2008. The LREW and its corresponding soil moisture probes network are shown in Figure 1.

### 2.2. Land Surface Model Inputs

A summary of all the inputs used in this study is given in Table 1 and a brief discussion, along with the method of downscaling to the fine resolution (1/3 arc sec), is given below.

#### 2.2.1. Land Cover

The land cover data come from the 2006 National Land Cover Database (NLCD), a 16-class land cover classification at a spatial resolution of 30 m (∼1 arc sec) that spans the contiguous United States (CONUS) [*Fry et al*., 2011]. The NLCD data over LREW are downscaled to a 1/3 arc sec spatial resolution using nearest neighbor interpolation. The parameters associated with each land cover type come from the North American Land Data Assimilation System (NLDAS-2) [*Xia et al*., 2012].

The Leaf Area Index (LAI) for each grid cell is taken from the BNU-MODIS product, which provides estimates every 8 days at a 30 arc sec spatial resolution [*Yuan et al*., 2011]. Due to model structure limitations of using a temporally varying LAI, a monthly climatology calculated from this data set (2000–2009) is used instead.

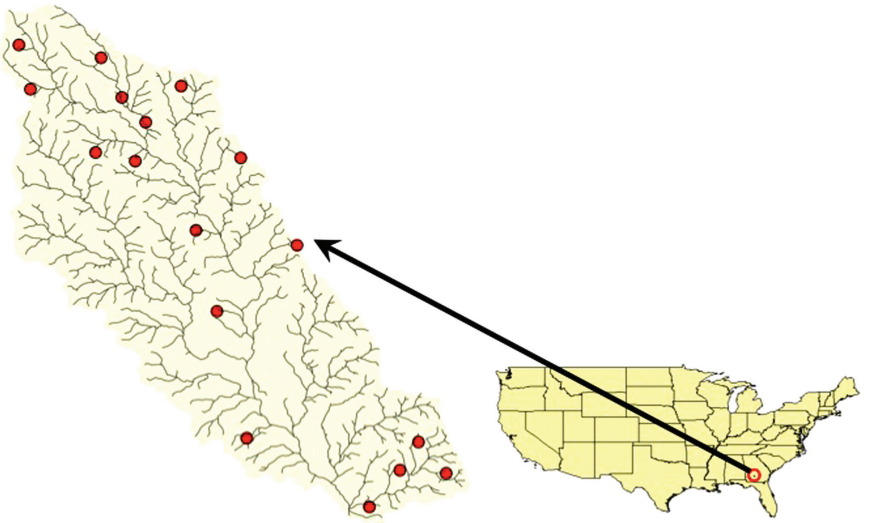

**Figure 1.** The Little River Experimental Watershed (334 km$^2$) in Georgia is part of the headwaters of the Suwanee river basin. It is characterized by a humid subtropical climate, loamy soils, and mainly crop production. As part of the USDA-ARS Southeast Watershed Research it hosts a network of 17 soil moisture probes distributed throughout the catchment.

The monthly climatology LAI is downscaled to the fine resolution using the land cover data set and the NOAH land surface model look-up table and rescaling the 30 arc sec grid cell mean to match the BNU-MODIS values. A monthly climatology is chosen to minimize biases and random errors from finer temporal scales.

### 2.2.2. Soil Properties

The soil properties come from the SSURGO database [*Soil Survey Staff*, 2012]. The average spatial coverage of each SSURGO map unit is around 80,000 m$^2$. For each map unit, the soil hydraulic properties are set to be a weighted mean of representative values of each of the unit's components. The soil properties are then downscaled to the 1/3 arc sec using nearest neighbor interpolation. Finally, a set of Pedotransfer functions [*Maidment*, 1993] are used to derive the missing soil hydraulic properties (residual soil moisture and the Brooks-Corey parameters) by using the soil texture from SSURGO.

### 2.2.3. Topography

The 1/3 arc sec USGS National Elevation Dataset DEM [*Gesch et al*., 2009] is used to delineate the watershed and derive the soils-topographic index. We use the MATLAB$^{TM}$ TopoToolbox [*Schwanghart and Kuhn*, 2010] to calculate the steepest downward gradient of each pixel's eight connected neighbors and the D-infinity algorithm to calculate the flow accumulation [*Tarboton*, 1997]. This information is combined with the soil properties and TOPMODEL's linear reservoir parameter to construct the soils-topographic index STI$=\ln\left(\frac{aT_0}{\tan\beta T_e}\right)$ over the basin [*Sivapalan et al*., 1987]. The soils-topographic index is computed from the specific catchment area $a$, local maximum transmissivity $T_0$, local slope $\beta$, and catchment averaged maximum transmissivity $T_e$. This index differs from the classic topographic index [*Beven and Kirby*, 1979] by introducing the influence of soil heterogeneity through the local maximum transmissivity at each grid cell.

**Table 1.** Data Sets (Native Spatial and Temporal Resolution) Used to Drive the TOPLATS Hydrologic Model Over the Little River Experimental Watershed

| Data Type | Data Set | Temporal Resolution | Spatial Resolution | Citation |
|---|---|---|---|---|
| Land cover | NLCD 2006 | N/A | 30 m | *Fry et al*. [2011] |
| | MODIS-BNU | 8 day | 30 arc sec (~1000 m) | *Yuan et al*. [2011] |
| Soil properties | SSURGO | N/A | ~80,000 m$^2$ | *Soil Survey Staff* [2012] |
| Topography | USGS-NED | N/A | 1/3 arc sec (~9 m) | *Gesch et al*. [2009] |
| Meteorology | NLDAS-2 | 1 h | 1/8° (~12,000 m) | *Xia et al*. [2012] |
| Precipitation | Stage IV | 1 h | 4000 m | *Lin and Mitchell* [2005] |
| | USDA | 1 h | N/A | *Bosch et al*. [2007] |

#### 2.2.4. Meteorology

The model's meteorological forcing data (except for precipitation) are provided by the NLDAS-2 [*Xia et al*., 2012] data system. This data set uses observations to bias-correct shortwave radiation and surface meteorology reanalysis at a 1/8° spatial resolution and 1 h temporal resolution. The 1/8° downward shortwave and longwave radiation, relative humidity, pressure, air temperature, and wind speed are downscaled within the hydrologic model using nearest neighbor interpolation to 1/3 arc sec.

Due to the strong influence of precipitation on the soil moisture heterogeneity, effort is taken to ensure that a high-quality precipitation product is used. The precipitation data come from using bilinear interpolation to downscale NCEP's Stage IV radar product (4 km) to a 15 arc sec (∼500 m) spatial resolution. The downscaled fields are then bias corrected with available USDA rain gauges by using the technique outlined in *Chaney et al*. [2014] at a 1 h time step. This method is equivalent to using simple Kriging to interpolate the absolute departures ($d = x_{gauge} - x_{radar}$) at each time step and superimpose the interpolated departures field on the original radar rainfall field to arrive at an improved estimate. In the downscaling and bias correction 15 arc sec was chosen, instead of 1/3 arc sec, to minimize storage and maximize computation efficiency in the bias correction. The 15 arc sec rainfall field is further downscaled within the hydrologic model to the 1/3 arc sec using nearest neighbor.

The spatial variability of rainfall at time scales on the order of minutes cannot be captured using downscaled precipitation with an effective resolution of 15 arc sec, however, the primary focus of this study is at the hourly to daily time scales. *Ciach and Krajewski* [2006] and *Villarini et al*. [2008] show for sites in Oklahoma and the United Kingdom how the spatial correlation of rainfall is very high at the 1 h and especially daily time scales at a 500 m spatial resolution. This justifies simulating and analyzing the 1/3 arc sec soil moisture spatial patterns at this temporal scale without using an equally detailed rainfall product.

## 3. Methodology

### 3.1. TOPLATS: Land Surface and Hydrologic Model

TOPLATS combines a TOPMODEL framework [*Beven and Kirby*, 1979] with a SVAT (soil vegetation atmosphere transfer scheme) making it suitable for high-resolution land surface modeling while maintaining computational efficiency. For a detailed background of the current version of TOPLATS, see *Sivapalan et al*. [1987], *Famiglietti and Wood* [1994], *Peters-Lidard et al*. [1997], and *Pauwels and Wood* [1999], however, a brief overview of the model's features applicable to this study is given below.

The water and energy balance are solved for each grid cell in order to generate a spatial distribution of water table depth, soil moisture, surface temperature, and fluxes. The land surface is partitioned into bare-soil and vegetated components. A single layer canopy covers each vegetated grid cell uniformly. The subsurface is divided into two layers: an upper active root zone and a lower less active transmission zone. The thin upper layer zone supplies water for bare soil evaporation, while water for vegetation transpiration can be supplied by either or both layers, depending on the distribution of the roots in the soil column. The water table depth used for each grid cell SVAT is controlled through the coupling with TOPMODEL. Surface runoff is created by both infiltration and saturation excess mechanisms.

The TOPMODEL framework allows for a dynamic yet computationally efficient redistribution of the groundwater from topographic and soil texture variability throughout the catchment using the soils-topographic index [*Sivapalan et al*., 1987]. This allows for the depiction of the control of topography on the spatial variability of soil moisture and surface fluxes. The catchment's base flow is modeled as an exponential decay as a function of the catchment's mean water table depth.

### 3.2. Model Performance: Calibration and Equifinality

#### 3.2.1. Latin Hypercube Sample

To both obtain optimal model performance while assessing the role of model parameter uncertainty the Latin hypercube sampling technique (LHS) [*McKay et al*., 1979] is used to assess model performance across the model parameter space. The LHS is used to generate 1000 parameter sets by sampling (assuming uniform distributions) from three parameters: saturated base flow ($Q_{b0}$), base flow exponential decay parameter (f), and root zone depth (uniform over the catchment). For each parameter set, January to June 2004 is used for spin-up of the hydrologic model, July 2004 to December 2006 for calibration, and January 2007 to

December 2008 for validation. A multiobjective function is used to assess model performance against the daily time series of network soil moisture spatial mean and spatial standard deviation of in situ soil moisture measurements. The model's implementation of only two soil layers dictates a comparison of the arithmetic average of the 5, 20, and 30 cm probes to the root zone soil moisture. The multiobjective performance metric combines the Kling-Gupta Efficiency (KGE) [*Gupta et al*., 2009] of the time series of simulated network (colocated grid cells) soil moisture spatial mean and spatial soil moisture standard deviation; in an equally weighted linear combination.

$$KGE = 1 - \sqrt{\left(r_{pearson} - 1\right)^2 + \left(\frac{\sigma_{model}}{\sigma_{obs}} - 1\right)^2 + \left(\frac{\mu_{model}}{\mu_{obs}} - 1\right)^2}$$

$$KGE_{comb} = \frac{KGE_{mean} + KGE_{std}}{2}$$

#### 3.2.2. Stratified Sampling Model Reduction (SSMR)

Running TOPLATS in fully distributed mode at a 1/3 arc sec resolution over the LREW (>3 million grid cells) for the 1000 LHS parameter sets presents a unique computational challenge. Simplifying the model while retaining the statistical properties of the 1/3 arc sec grid is essential. One possibility is to follow the classic TOPMODEL framework and model the distribution of 1/3 arc sec soils-topographic index. However, TOPLATS accounts for not only distributed topography but also distributed soil, vegetation, and precipitation, making the statistical representation of the soils-topographic index too simplified to find optimal parameter sets that are applicable to the fully distributed model. Instead, we use a stratified sampling model reduction approach (SSMR) to capture the distribution of subsurface, surface, and land cover properties over the catchment while still accounting for the meteorological spatial distribution. The chosen grid resolution is 5 arc sec, which gives 225 times reduction in the number of grid cells. For each 5 arc sec grid cell, a random 1/3 arc sec grid cell is sampled as part of the calibration. Because the calibrated parameters are catchment parameters, and not individual grid cell parameters, as long as the coarser grid is statistically representative of the fine scale, the skill of the optimal parameter sets of the coarser grid should apply at finer scales. To ensure an equal comparison of each soil moisture probe to its colocated fine-scale grid cell, the corresponding coarse grid cell is fixed to have the properties of the colocated fine-scale grid cell.

### 3.3. Controls on the Spatial Variability of Soil Moisture

To assess the influence of each driver of heterogeneity on the spatial variability of soil moisture over the LREW, we perform a number of controlled experiments. The initial experiment consists of spatially uniform topography (mean soils-topographic index), precipitation (catchment mean), soil properties (most frequent soil texture), and vegetation (most frequent land cover type). In this simulation, only heterogeneity in non-precipitation meteorology is present. Other simulations consist of adding the heterogeneity of each variable one at a time. The importance of each driver is assessed by comparing the standard deviation of the root zone soil moisture over the catchment and the simulated network at each time step to that of the baseline simulations (all heterogeneity) and the soil moisture probes.

### 3.4. Network Design

The strong relationship between soil moisture areal mean and areal variance suggests that robust network upscaling relies on the network configuration; it must accurately capture the time varying areal variance. Most studies of soil moisture heterogeneity using in situ measurements have used a stratified grid at a spatial resolution between 10 and 100 m [*Crow et al*., 2005; *Mohanty et al*., 2000; *Western et al*., 1998]. To capture the drivers of heterogeneity, a stratified grid has also been combined with simple random sampling [*Rosenbaum et al*., 2012] or topographic gradients [*Vivoni et al*., 2010; *Wilson et al*., 2005]. *Bircher et al*. [2012] used multiple clusters of fine-scale networks to account for precipitation gradients. For each fine network, GIS data sets were used to determine the most representative land units in which to place the ground measurements. This approach follows *Friesen et al*. [2008] that uses elevation, topographic sequence, soil type, slope, land use, and aspect to define landscape units that show consistent hydrologic behavior (hydrotopes).

A similar approach to *Friesen et al*. [2008] is to combine the concepts of landscape units and hydrologic similarity to define similar behaving fine-scale grid cells through hydrologic similar units (HSUs) [*Page et al*.,

**Table 2.** Results From 1000 Latin Hypercube Sample 5 Arc Sec TOPLATS Simulations Over the Little River Experimental Watershed

| $KGE_{comb}$ | | Number of Parameters Sets Above $KGE_{comb}$ Threshold | | | | |
|---|---|---|---|---|---|---|
| Best | Mean | 0.0 | 0.25 | 0.50 | 0.60 | 0.70 |
| 0.730 | −0.049 | 426 (42.6%) | 256 (25.6%) | 59 (5.9%) | 39 (3.9%) | 5 (0.5%) |

2007]. Assuming that the TOPLATS simulated soil moisture fields over the LREW reflect the ground truth, we use hydrologic similar units (HSUs) to develop an in situ network design technique that accurately captures the heterogeneity of soil moisture by relying exclusively on proxies of the static drivers of spatial heterogeneity (soils-topographic index, saturated water content, and land cover type) to define the HSUs. These proxies can be extracted from high-resolution GIS data sets where available.

Complex interactions between the land surface components result in significant differences in the temporal evolution of soil moisture among HSUs. As a result, network design should focus on capturing the different types of HSUs throughout the catchment. This is accomplished by clustering the drivers of heterogeneity through a three-dimensional histogram (soils-topographic index, saturated water content, and land cover type). Each bin of the 3-D histogram represents an HSU. The percentage of the catchment covered by the HSU defines its relevance among other HSUs. The main challenge is to determine the appropriate binning since the goal is for a hydrologic similar unit to be representative (within approximation) of all grid cells within the bin. If available, information regarding the role of each driver of heterogeneity can guide the histogram binning. The probes are placed by randomly sampling one grid cell (and only one grid cell) from each hydrologic similar unit (3-D histogram bin). The histogram values (percentages) are used to construct the catchment mean and standard deviation by acting as weights for each HSU's soil moisture values.

The proposed new sampling method accounts for all hydrologic similar units while keeping the sample size small; sampling only one grid cell per HSU and minimizing the number of HSUs (bins). To understand the sensitivity of this sampling method on reproducing the mean and standard deviation of the catchment, multiple three-dimensional histograms are considered. The different three-dimensional histograms are constructed by adjusting the number of bins of the soils-topographic index (nt = 1, 2, 3, 5, 10, 15, and 20), saturated soil water content (ns = 1, 2, 3, 5, 10, 15, and 20), and land cover type (nv = 1, 2, 5, 10, and 14). This leads to 245 different histograms. The network is then constructed by sampling at random a grid cell (and only one grid cell) that belongs to each bin. We use 100 networks for each of the 245 histograms to assess the uncertainty of random sampling within each bin.

## 4. Results

### 4.1. Model Performance: Calibration and Equifinality

#### 4.1.1. Latin Hypercube Sample

The Latin Hypercube Sampling scheme is applied to run TOPLATS with 1000 representative parameter sets. For each of the simulations the performance metric ($KGE_{comb}$) described in section 3.2.1 is computed. In all cases, for each time step a probe's colocated grid cell value is used to compute the mean and standard deviation if the probe reports a value. Table 2 shows the top performance in the sampled parameter space ($KGE_{comb} = 0.730$), the mean performance of all parameter sets, and the number of sets that meet certain performance criteria. Assuming a $KGE_{comb}$ of 0.5 as the acceptable parameter set criteria, 5.9% of the model simulations are equally plausible solutions.

The distribution of $KGE_{comb}$ is then used to determine how the performance changes when using other metrics (NSE, RMSE, MAE, and $R^2$) to compare each of the 1000 simulations simulated network mean and standard deviation. The analysis is extended to cover both the calibration (July 2004 to December 2006) and validation periods (January 2007 to December 2008). As shown in Table 3, in general, all metrics show an increase in performance as one moves toward the higher percentiles in the $KGE_{comb}$ distribution. The standard deviation sees a larger decrease in performance than the mean when comparing the validation period to the calibration period. There are cases when the higher $KGE_{comb}$ leads to a decrease in other metrics (e.g., NSE of the mean soil moisture) reinforcing the need to account for parameter uncertainty when analyzing the simulations with the optimal parameter sets according to the $KGE_{comb}$.

**Table 3.** The Distribution (Best, Mean, and Percentiles) of the $KGE_{comb}$ (See Table 2) Is Used to Assess the Performance of the 1000 Latin Hypercube Sample 5 Arc Sec Simulations for the Calibration and Validation Periods Using a Suite of Metrics

| | | | Best | Mean | 25th | 50th | 75th | 90th | 95th | 99th |
|---|---|---|---|---|---|---|---|---|---|---|
| Mean | Calibration | KGE | 0.89 | 0.14 | 0.15 | 0.27 | 0.46 | 0.67 | 0.75 | 0.78 |
| | | NSE | 0.84 | −2.16 | −1.41 | −0.04 | 0.45 | 0.53 | 0.79 | 0.66 |
| | | RMSE | 0.02 | 0.06 | 0.06 | 0.04 | 0.03 | 0.03 | 0.02 | 0.02 |
| | | MAE | 0.01 | 0.05 | 0.06 | 0.03 | 0.02 | 0.02 | 0.02 | 0.02 |
| | | $R^2$ | 0.85 | 0.52 | 0.39 | 0.6 | 0.62 | 0.71 | 0.84 | 0.82 |
| | Validation | KGE | 0.85 | 0.11 | 0.22 | 0.34 | 0.2 | 0.68 | 0.74 | 0.68 |
| | | NSE | 0.77 | −2.59 | −0.37 | 0.34 | 0.02 | 0.67 | 0.79 | 0.5 |
| | | RMSE | 0.02 | 0.06 | 0.05 | 0.03 | 0.04 | 0.02 | 0.02 | 0.03 |
| | | MAE | 0.02 | 0.05 | 0.04 | 0.03 | 0.03 | 0.02 | 0.02 | 0.02 |
| | | $R^2$ | 0.83 | 0.51 | 0.22 | 0.69 | 0.5 | 0.72 | 0.81 | 0.81 |
| Standard deviation | Calibration | KGE | 0.57 | −0.24 | −0.67 | −0.5 | 0.05 | 0.15 | 0.4 | 0.59 |
| | | NSE | −0.19 | −4.39 | −11.88 | −5.91 | −0.99 | −1.86 | −0.37 | −0.1 |
| | | RMSE | 0.02 | 0.04 | 0.07 | 0.05 | 0.03 | 0.03 | 0.02 | 0.02 |
| | | MAE | 0.02 | 0.04 | 0.07 | 0.05 | 0.03 | 0.03 | 0.02 | 0.02 |
| | | $R^2$ | 0.76 | 0.26 | 0 | 0 | 0.55 | 0.32 | 0.72 | 0.71 |
| | Validation | KGE | 0.28 | −0.29 | −0.64 | −0.44 | −0.5 | −0.12 | 0.04 | 0.29 |
| | | NSE | −0.4 | −5.27 | −16.65 | −4.22 | −4.61 | −1.81 | −0.99 | −0.28 |
| | | RMSE | 0.02 | 0.04 | 0.07 | 0.04 | 0.04 | 0.03 | 0.02 | 0.02 |
| | | MAE | 0.02 | 0.03 | 0.06 | 0.03 | 0.03 | 0.02 | 0.02 | 0.02 |
| | | $R^2$ | 0.67 | 0.23 | 0.08 | 0 | 0 | 0.48 | 0.64 | 0.63 |

In the case of the NSE, the results suggest consistent poor performance of the standard deviation for all ensemble members. To understand this discrepancy, following the work of *Gupta et al.* [2009], the NSE values are decomposed into their three components $(NSE = 2\alpha r - \alpha^2 - \beta^2)$. Where $r$ is the linear correlation, $\alpha$ is the ratio between the standard deviation of the simulated and observed time series $\left(\alpha = \frac{\sigma_{model}}{\sigma_{obs}}\right)$, and $\beta$ is the ratio between the bias and the standard deviation of the observed time series $\left(\beta = \frac{\mu_{model} - \mu_{obs}}{\sigma_{obs}}\right)$. For the best parameter set in the TOPLATS simulations, according to the KGE metric, $r = 0.871$, $\alpha = 1.26$, $\beta = -0.89$. Since the bias term is divided by the standard deviation of the observed time series, a low coefficient of variation of the observed time series results in a high absolute value of $\beta$. This overwhelms the predictive power of the model to capture the temporal structure (e.g., seasonality) and variability (for more details see

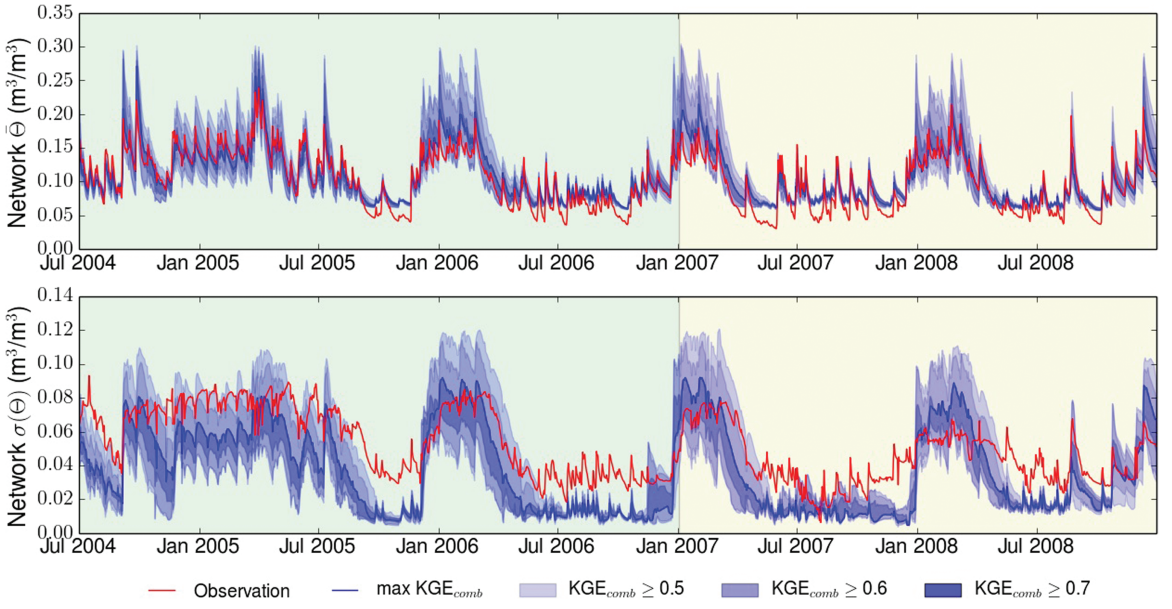


**Figure 2.** (top) The daily mean soil moisture of the probe's colocated grid cells, (bottom) and the daily standard deviation soil moisture of the probe's colocated grid cells from the TOPLATS simulations at a 5 arc sec spatial resolution compared to observations. The blue shading shows the spread of uncertainty among equally plausible parameter sets. The light green background defines the calibration period and the light brown background defines the validation period.

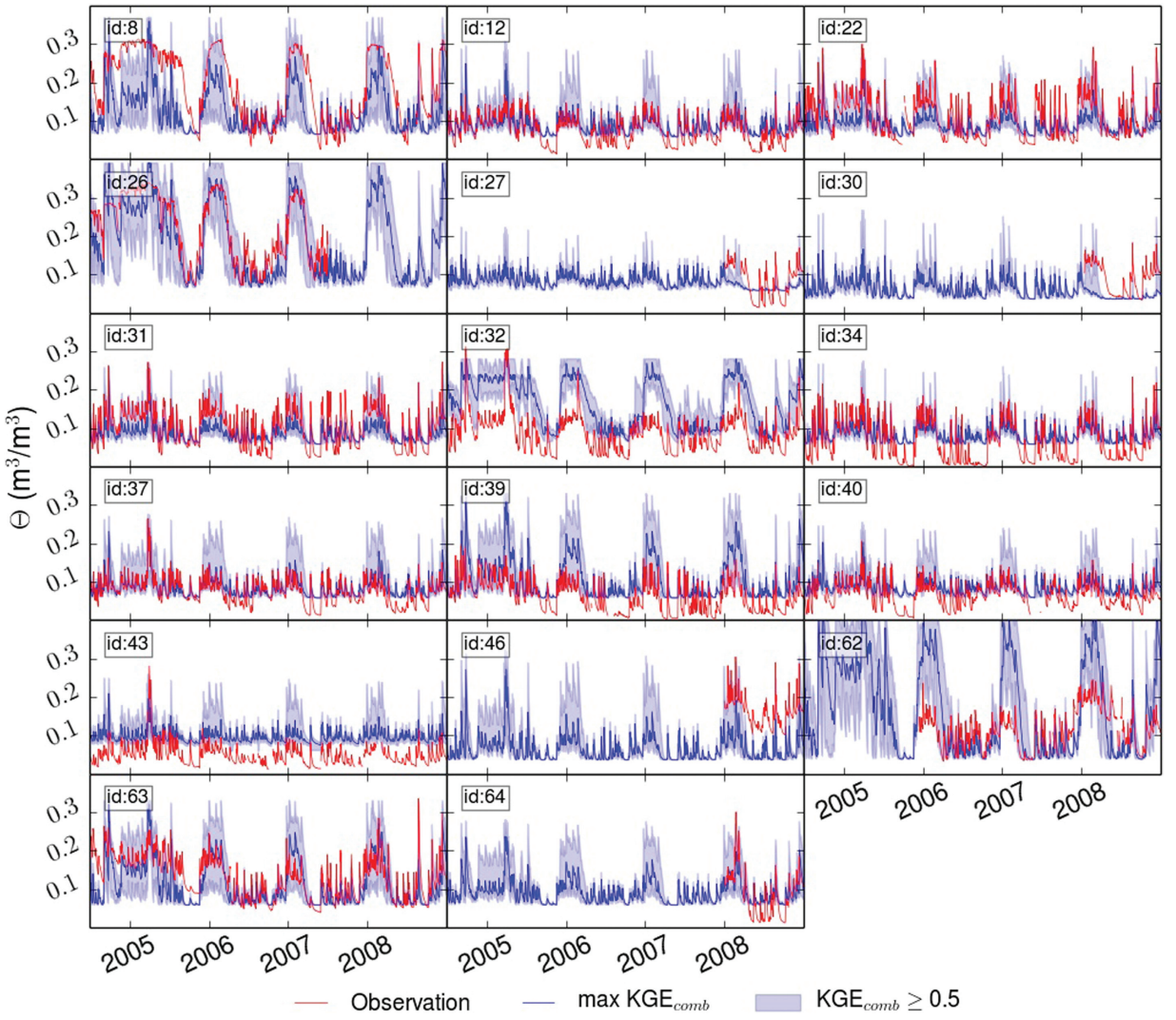


**Figure 3.** The daily soil moisture of the colocated grid cell from the TOPLATS simulations at a 5 arc sec spatial resolution compared to daily measurement from the probe. The blue shading shows the spread of uncertainty among equally plausible parameter sets.

*Gupta et al.* [2009]). The weaknesses of this normalized bias term are the primary reasons why the KGE is the primary metric used in this study.

Figure 2 compares the observed mean and standard deviation to the simulated network using all simulations with a $KGE_{comb} >= 0.5$. The mean shows a large ensemble spread during wet periods and a smaller spread during dry periods. The model shows a systematic bias during drier periods suggesting an exaggerated influence of saturated regions in the simulated network during these periods. The standard deviation also shows the largest spread during wet periods with a consistent lack of heterogeneity during dry periods while wet periods in many cases bound the observed heterogeneity. One encouraging outcome is that in all cases the simulated network captures the observed seasonality of heterogeneity suggesting that the model is accounting for the processes that drive the month-to-month variability of soil moisture heterogeneity over the network.

Although the model shows skill in capturing the dynamics of the LREW network's soil moisture mean and standard deviation, the ability to reproduce the individual in situ probes varies. Figure 3 shows the comparison between the in situ probes and their colocated grid cells between 2004 and 2008. For probes 8 and 26, topographic control allows the model to capture regions with extended periods of saturation. However, for probes 32 and 62 the topographic control leads to erroneous periods of high saturation. The errors at these

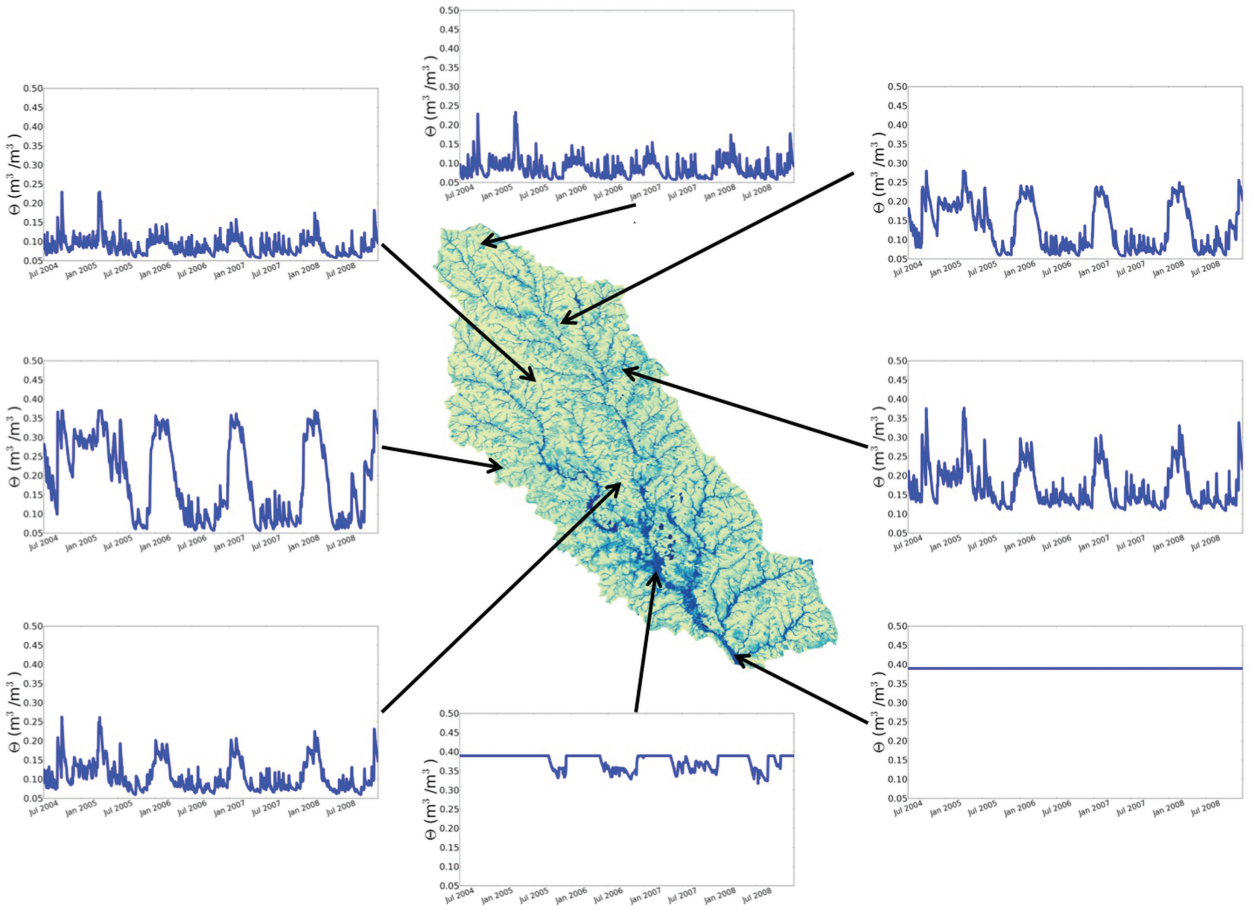

**Figure 4.** The daily averaged TOPLATS simulated soil moisture field at a 1/3 arc sec spatial resolution on 1 January 2007 over the Little River Experimental Watershed. The spatially varying temporal dynamics over the catchment is captured in the time series of root zone soil moisture of 8 distinct points in the catchment between July 2004 and December 2008.

two probes are most likely due to TOPMODEL's reliance on the soils-topographic index, derived flow paths, or random errors and biases in the DEM. For most probes, systematic biases are controlled by errors in soil hydraulic properties. For example, in some cases the low soil moisture values are considerably different than those seen by the probes. Although accounting for model catchment parameter uncertainty helps bound the observations at some sites, in most cases the ground truth cannot be captured in the acceptable model parameter space.

Given that the model results do not vary significantly across the acceptable parameter sets, we assume that the simulation using the best parameter set is suitable to represent the acceptable parameter space and use it for the remainder of this study. The parameter set that yields the highest performance has a uniform root zone depth of 45.60 cm, saturated base flow of 113.012 $m^3/s$, and base flow decay parameter of 6.25. Figure 4 shows an example spatial image of the modeled root zone soil moisture using the optimal parameter; also included is the temporal evolution at distinct points throughout the catchment.

#### 4.1.2. Stratified Sampling Model Reduction (SSMR)

Since this study relies on the assumption that the results using a coarser grid stratified sampling of the 1/3 arc sec grid cells are applicable at finer resolution, the derived optimal parameter set is tested on a number of grid scales. The model is run at 90, 30, 10, 3, and 1/3 arc sec spatial resolutions. We emphasize that the spatial resolution here is the grid at which the SSMR technique is applied. The KGE is computed between the 5 arc sec simulation and the other resolutions for the catchment mean and standard deviation of evapotranspiration, soil moisture, and surface runoff for all simulations between 2004 and 2008 at a daily time step. Figure 5 shows that the parameters found using the SSMR on a 5 arc sec grid are applicable to the

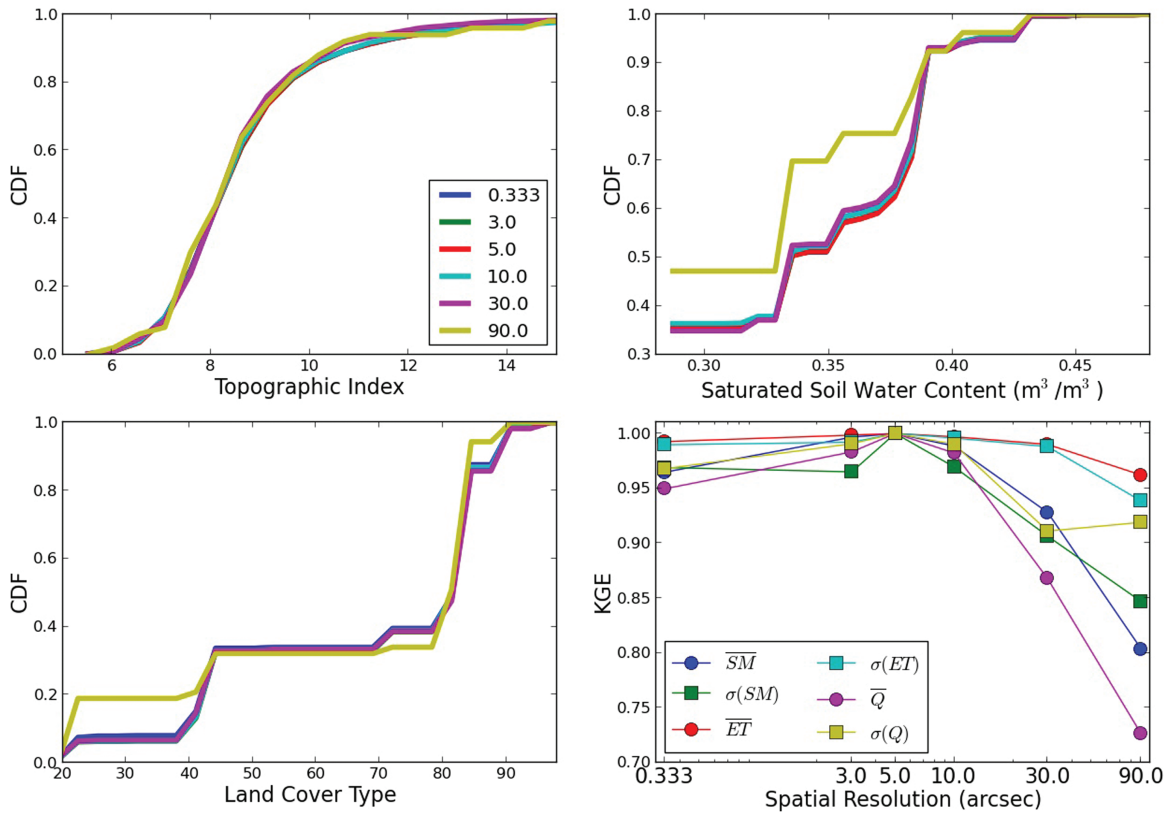


**Figure 5.** The TOPLATS model is run using the SSMR technique at a 0.333, 3, 5, 10, 30, and 90 arc sec spatial resolution. The KGE is used to compare the daily catchment mean and standard deviation of surface runoff, evapotranspiration, and root zone soil moisture to the 5 arc sec simulation (bottom right). The empirical cumulative distribution functions of proxies of the drivers of heterogeneity for (topography, top left) topographic index, (vegetation, bottom left) land cover type, (soil properties, top right) saturated soil water content are also compared.

model simulations between 1/3 and 10 arc sec. Above 10 arc sec the performance quickly deteriorates. This is explained in the comparison between the empirical cumulative distribution functions for proxies of land cover (land cover type), topography (topographic index), and soil properties (saturated soil water content) in Figure 5. When the sampling of the 1/3 arc sec is sufficiently large, the SSMR technique is able to capture the fine-scale simulated heterogeneity. However, when this assumption is no longer met, the model performance quickly deteriorates especially for surface runoff and soil moisture.

Acknowledging that uncertainties still exist in the calibrated model output, it is argued that the 1/3 arc sec simulated soil moisture fields are the best source of spatial soil moisture data for the Little River Experimental Watershed due to the more complete characterization of topography, soil properties, and vegetation and are used as ground truth for the remainder of the study. Due to the size of the 1/3 arc sec simulations ($>$50 gb, $>$10 days to run on a eight core machine), the analysis at the 1/3 arc sec resolution becomes impractical. As a result, the remaining model simulations and analysis are performed using the optimal 5 arc sec parameter set while assuming that the results scale down to the 1/3 spatial resolution.

### 4.2. Controls on the Spatial Variability of Soil Moisture

#### 4.2.1. Controlled Experiments

Understanding the controls of spatial variability of soil moisture is important for model development and assessment. The TOPLATS framework allows for an assessment and attribution of this variability by progressively adding sources of spatial variability to the model. The times series of the standard deviation of soil moisture of the networks' probes with the simulated network (colocated grid cells) and the entire simulated catchment are given in Figure 6. The different drivers of heterogeneity as described in section 3.3 are discussed in detail below.

1. M—All spatial heterogeneity removed, including for precipitation. Heterogeneity in other meteorological fields is retained. The spatial heterogeneity of soil moisture is negligible and is not seen in Figure 6 as it

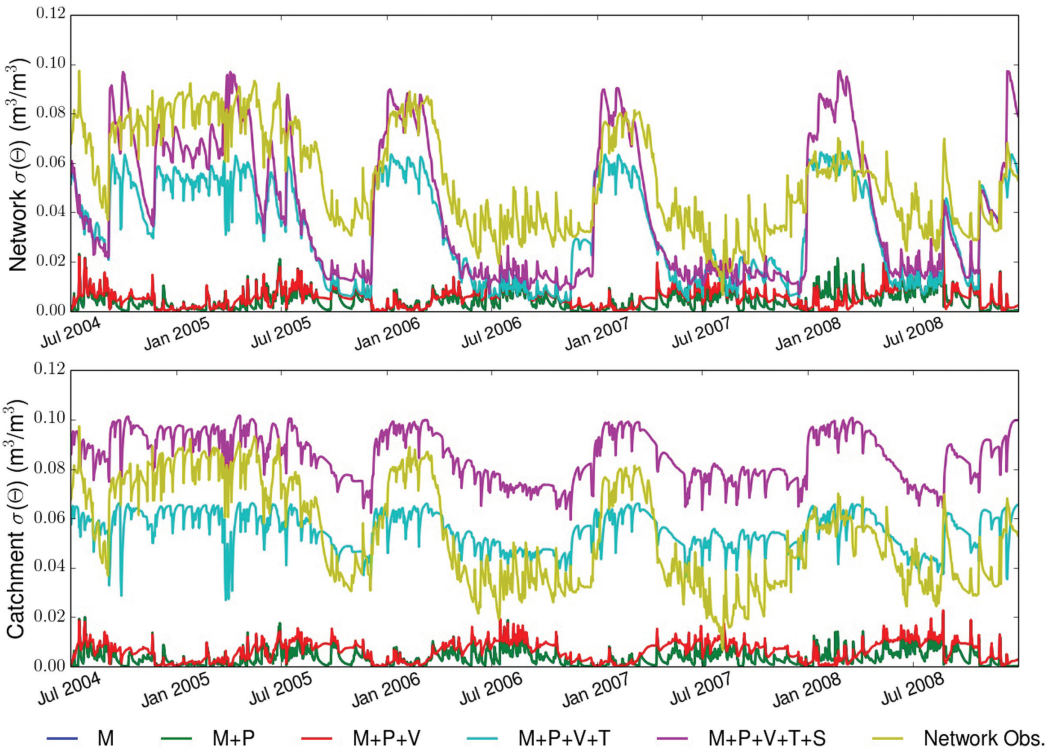


**Figure 6.** (top) The standard deviation of the probes and colocated grid cells and (bottom) the catchment for five TOPLATS simulations run at a 5 arc sec spatial resolution progressively adding heterogeneity: heterogeneity in meteorological inputs except precipitation (M), heterogeneity in precipitation (P), heterogeneity in vegetation (V), heterogeneity of topography (T), and heterogeneity of soil properties (S).

is practically a straight line at 0.0. The effective spatial resolution of the meteorology (450 arc sec) is not adequate to assess the impact of heterogeneity of radiation. In addition, comparing daily averages further dampens any spatial heterogeneity.

2. M + P—Add spatial heterogeneity of precipitation (15 arc sec): spikes in spatial heterogeneity appear after each storm, although the spikes decrease rapidly. There is also a higher spatial heterogeneity in the summer that is likely driven by an increase in rainfall heterogeneity from increased convection. Furthermore, the difference between the simulated network and the entire catchment is negligible, suggesting that the network captures the spatial variability. Although the variability in precipitation added to the spatial variability of soil moisture there is still a large discrepancy between the model and the observations.

3. M + P + V—Add spatial heterogeneity of land cover (1 arc sec): the addition of the spatial variability of vegetation amplifies the seasonal cycle during the summer months. During the summer, the spatial heterogeneity in evapotranspiration from the different land cover types drives the increase in heterogeneity. During the winter there is less heterogeneity in the vegetation and less evapotranspiration and therefore less control of spatial variability of soil moisture. The seasonal cycle is also more significant at the catchment scale. This is likely due to the under sampling of the vegetation heterogeneity of the probes. It is also interesting that the seasonal cycle is negatively correlated to the probes' standard deviation. This suggests that there are key controls to the spatial variability of the soil moisture that are not represented in precipitation and vegetation alone.

4. M + P + V + T—Add spatial heterogeneity of topography (1/3 arc sec): there is a large increase in the spatial variability of the soil moisture due to the addition of topography, particularly during the winter. Furthermore, the seasonal cycle is now positively correlated with the in situ network. This can be explained by the connection between topography and the water table assumed in the model. During summer, the water table is sufficiently low that the effects of topography are negligible. (Note that most of the heterogeneity can be explained during these months by evapotranspiration spatial patterns.) During winter, the water table is closer to the surface allowing topography to control heterogeneity over the in situ

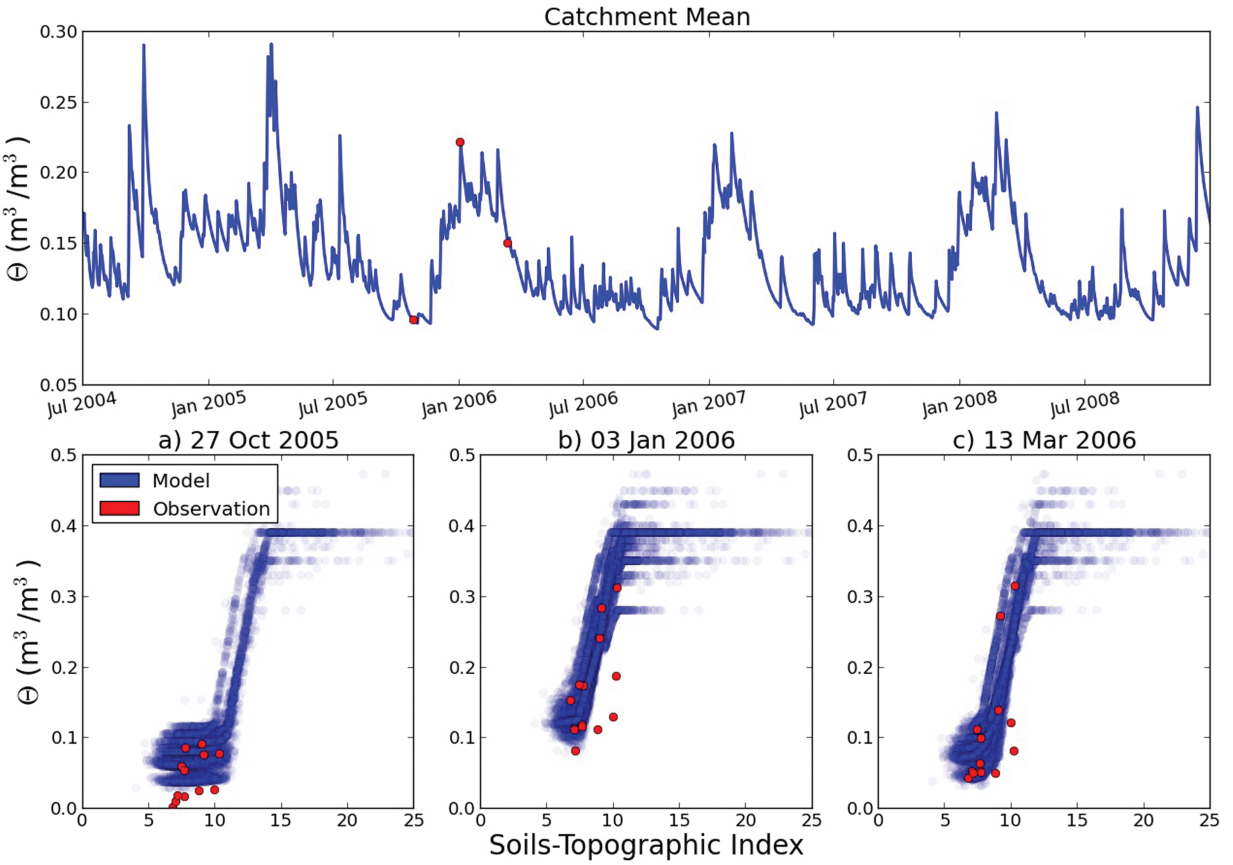


**Figure 7.** (top) The catchment mean soil moisture time series and (bottom) grid-scale relationship of soil-topographic index with model and observed soil moisture for (a) dry, (b) wet, and (c) transitional regime for the LREW.

network's colocated grid cells. The catchment heterogeneity is significantly higher than the network's during the summer.

5. M + P + V + T + S—Add spatial heterogeneity of soil properties (~80,000 $m^2$): the addition of heterogeneity of the soil properties shows an increase in the spatial variability of soil moisture. This increase is uniform and shows no impact on the seasonality of the heterogeneity of soil moisture. Including all drivers of spatial heterogeneity in the model leads to a more accurate representation of the network's seasonality of the soil moisture standard deviation. These controlled experiments suggest topography is the main control of heterogeneity in the network's colocated grid cells in the wintertime. In comparison, the vegetation heterogeneity is the main control during the summer. Systematic biases in the standard deviation still remain after adding all the analyzed sources of heterogeneity.

#### 4.2.2. Relationship Between Soil Moisture and the Soils-Topographic Index

It is possible that TOPLATS overemphasizes the role of topography in soil moisture heterogeneity. To test whether the previous results are an artifact of the model or are connected to the observations, we analyze the time varying relationship between the soils-topographic index and the modeled and observed soil moisture. Figure 7 shows this relationship for three distinct periods: dry, transitional, and wet. The linear relationship (transition regime) between the dry and saturated soil moisture values is a product of TOPMODEL theory. For the dry case (27 October 2005), most of the modeled grid cells in the watershed are between their respective wilting and residual soil moisture values with few areas in the transition and saturated regimes. During this period, the observations only report dry values; this helps understand the decrease in observed heterogeneity during dry periods (see Figure 6). For the wet case (3 January 2006) the saturation occurs at lower soils-topographic indices and the rest of the catchment is in the transition zone. Similar to the model, all the observations have left the dry cluster and are now in the transition regime. In

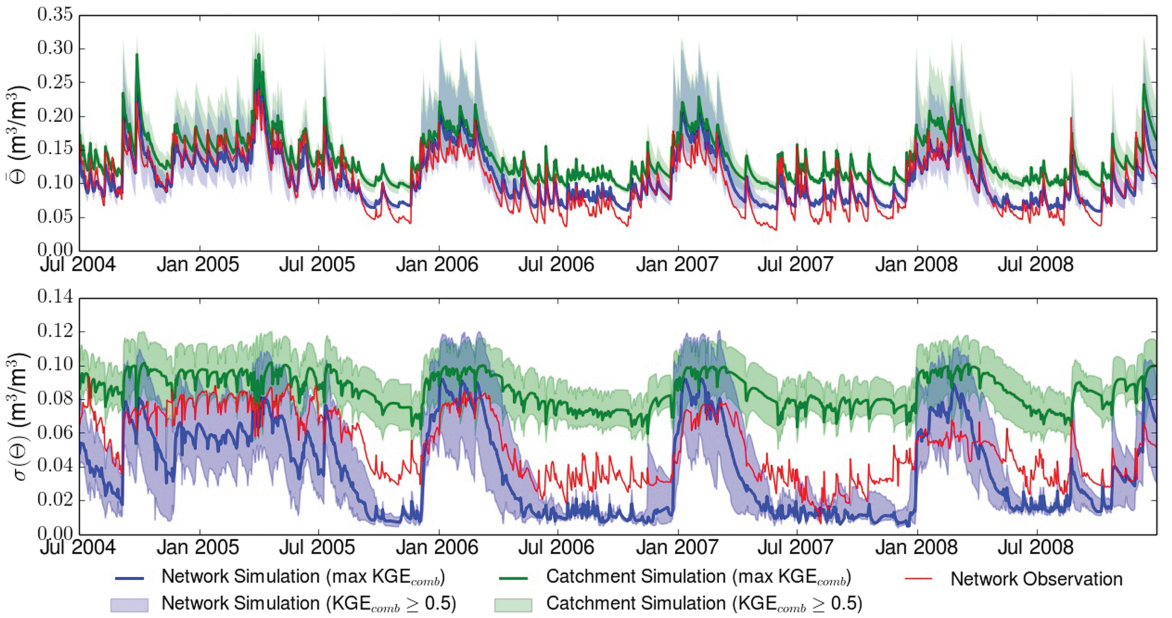


**Figure 8.** The TOPLATS simulated catchment and network mean and standard deviation of soil moisture at a 5 arc sec spatial resolution compared to the LREW observation network. The blue and green shading show the spread of uncertainty among equally plausible parameter sets.

the transition case (13 March 2006), there is a decrease in saturation and a significant increase in dry areas. Most of the observations have already entered the dry cluster while a few remain in the transition regime. These results suggest the model captures the general dynamics of the observations while raising the question of whether the number of modeled saturated grid cells not captured by the observations is a model artifact or a deficiency in the existing network configuration.

### 4.3. Network Design

Figure 8 compares the simulated catchment mean and standard deviation to the simulated and observed network. The results suggest that the current (simulated and observed) network of soil moisture probes underestimates the spatial standard deviation and mean as compared to the catchment simulations (also apparent in Figure 7). The results are very similar when using the entire ensemble of simulations of acceptable parameters ($KGE_{comb} >= 0.5$). Although the TOPLATS model probably exaggerates saturated regions (see Figures 2 and 3), the most likely physical explanation of the discrepancy in Figure 8 is an inadequate sampling of wet regions (probes are not located in floodplains, lakes, or streams) by the existing network; instead it emphasizes transition or dry regions. The differences are more appreciable during the dry period when land cover heterogeneity controls the simulated network's soil moisture heterogeneity while the soils-topographic index (topography and soils) controls the catchment's soil moisture heterogeneity.

In order to determine if the lack of probes in wet areas is under-sampled in the existing network, an exhaustive analysis of all possible combinations of probes in a network ($n \leq 17$) is explored. As shown in Figure 9, the temporal average catchment mean and standard deviation is higher than the simulated and observed network for almost all possible network combinations constructed from subsets of the existing network. The results are most dramatic for the case of the standard deviation, where the average values of the possible networks are significantly lower that the catchment estimate. These results substantiate the results shown in Figure 8; a lack of probes in wet regions leads to an underestimation, especially in the dry periods, of the catchment mean and standard deviation.

For a reconfigured network to accurately capture the catchment mean and heterogeneity, all the drivers of spatial heterogeneity in the catchment must be represented in the network. As shown previously, the main drivers of heterogeneity in the LREW catchment are topography, soil properties and vegetation. Proxies of these drivers are shown in Figure 10 in a three-dimensional histogram of the soils-topographic index, saturated water content, and land cover type. Each bin represents a unique hydrologic similar unit in the

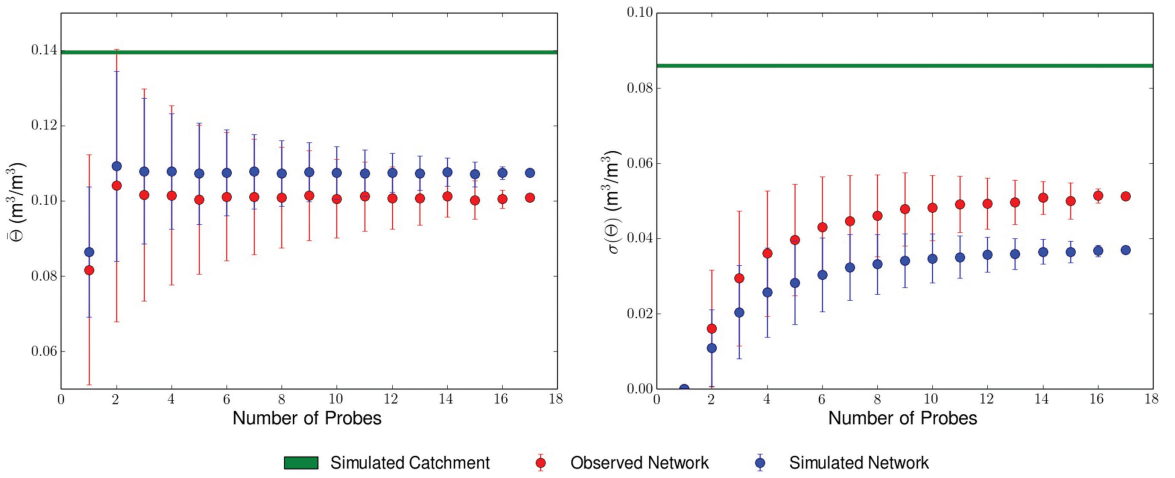


**Figure 9.** Assessment of the existing LREW network's ability to reproduce the average TOPLATS catchment mean and standard deviation (green). All combinations for a given number of probes are used to construct a network for both the observed (red) and simulated networks (blue).

catchment for which the most frequent features are mid to low soils-topographic indices, low saturated water content, and croplands. Due to the high frequency of some units, simple random sampling of the catchment will on average give preference to these HSUs, regardless of how representative they are of the entire catchment. The proposed sampling method samples one grid cell from each HSU and the 3-D histogram informs how relevant that sample is among samples from other HSUs.

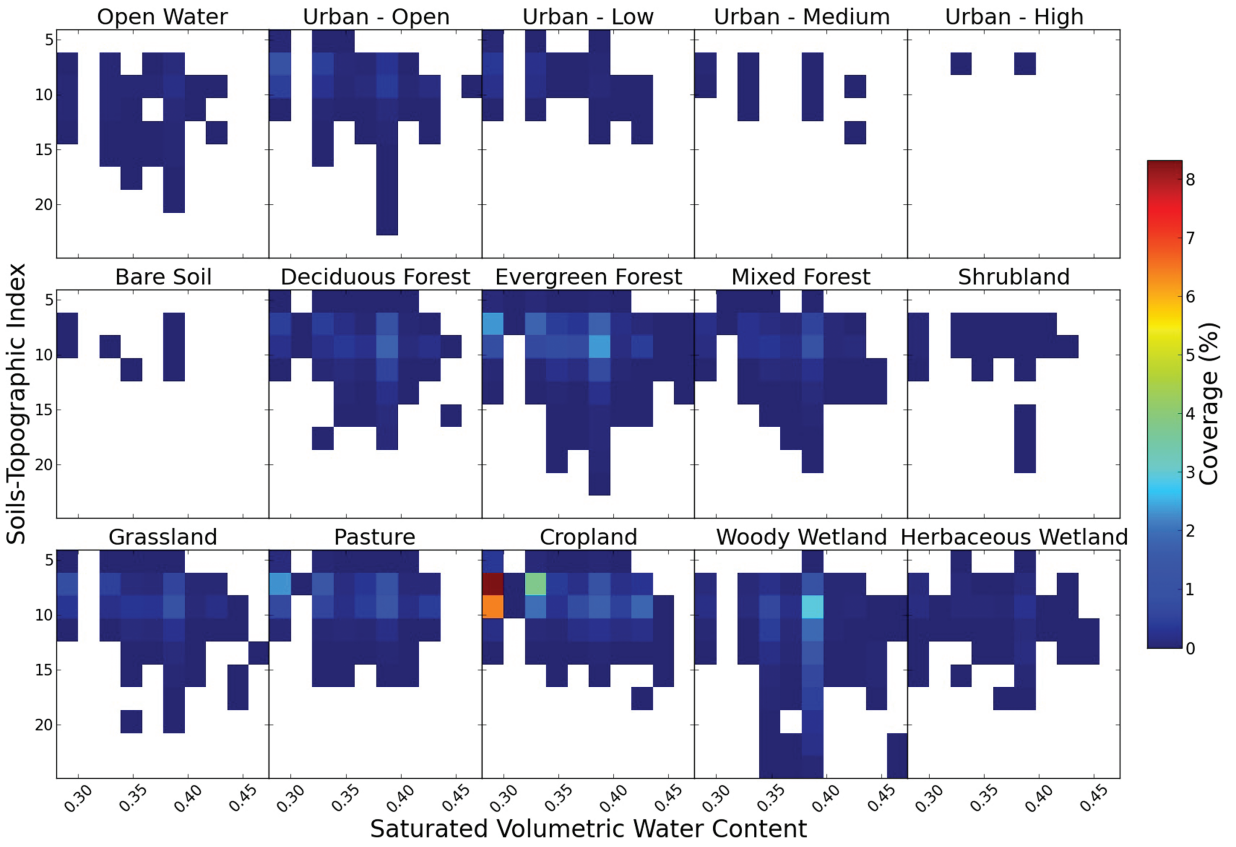


**Figure 10.** The percentage coverage of unique hydrologic similar units within the LREW derived from soils-topographic index, saturated volumetric water content, and land cover type as proxies of topography, soil properties, and vegetation.

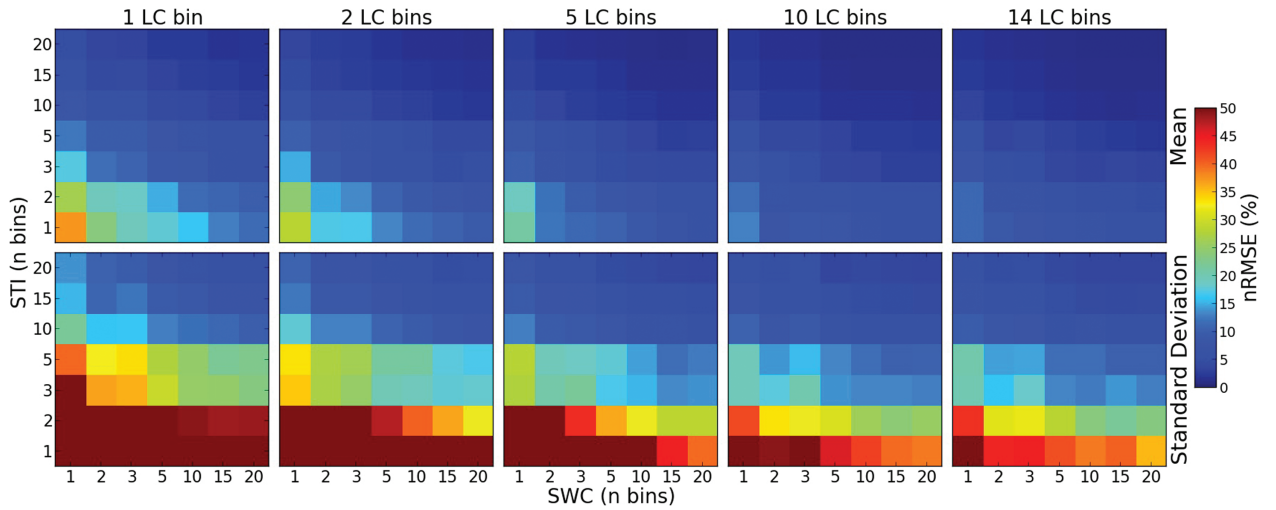


**Figure 11.** The mean normalized root mean squared error (nRMSE) between the catchment and simulated network for the (top) mean and (bottom) standard deviation for networks sampled from different 3-D histograms based on the number of bins of soils-topographic index (STI), saturated volumetric water content (SWC), and land cover type (LC).

To understand the sensitivity of the new sampling method to reproduce the mean and standard deviation of the catchment, multiple three-dimensional histograms are considered (see section 3.4, for details). The average performance of the networks constructed from each of the 245 histograms is assessed in Figure 11 by showing the averaged normalized root mean squared error (nRMSE) of the new networks' time series of mean and standard deviation with respect to the catchment's synthetic truth (5 arc sec TOPLATS simulations). These results suggest that at low network densities, trading vegetation and soil bins for a higher number of soils-topographic bins leads on average to lower errors. The results are especially apparent when trying to reduce the error of the estimated spatial standard deviation.

To assess how the 3-D histogram sampling method compares to simple random sampling the two are compared for a given number of stations (1, 2, 3, 5, 10, 20, 50, 100, 200, and 500). To assess sampling uncertainty, 100 networks are used for each method for a given number of stations. For the 3-D histogram method, the binning for a given number of stations is chosen from the optimal path (histogram configuration) from Figure 11. Optimality is defined as the minimum of the weighted average of the mean nRMSE of the mean and standard deviation for a given number of stations (nonempty bins).

The comparison results are shown in Figure 12. At 1 station, the 3-D histogram is simple random sampling explaining the equal performance (differences are due to only sampling 100 networks). After that point, the

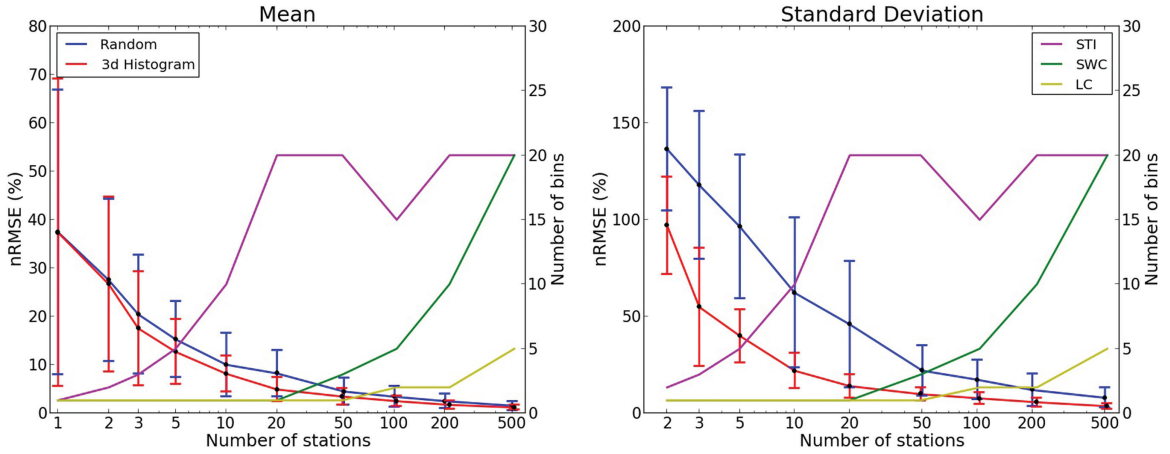


**Figure 12.** Comparison between the 3-D histogram sampling approach (optimal path) and simple random sampling. Performance is assessed by the normalized root mean squared error for both the (left) catchment mean and (right) standard deviation. The number of bins for each of the drivers as a function of the number of stations used in the optimal path 3-D histogram is also shown.

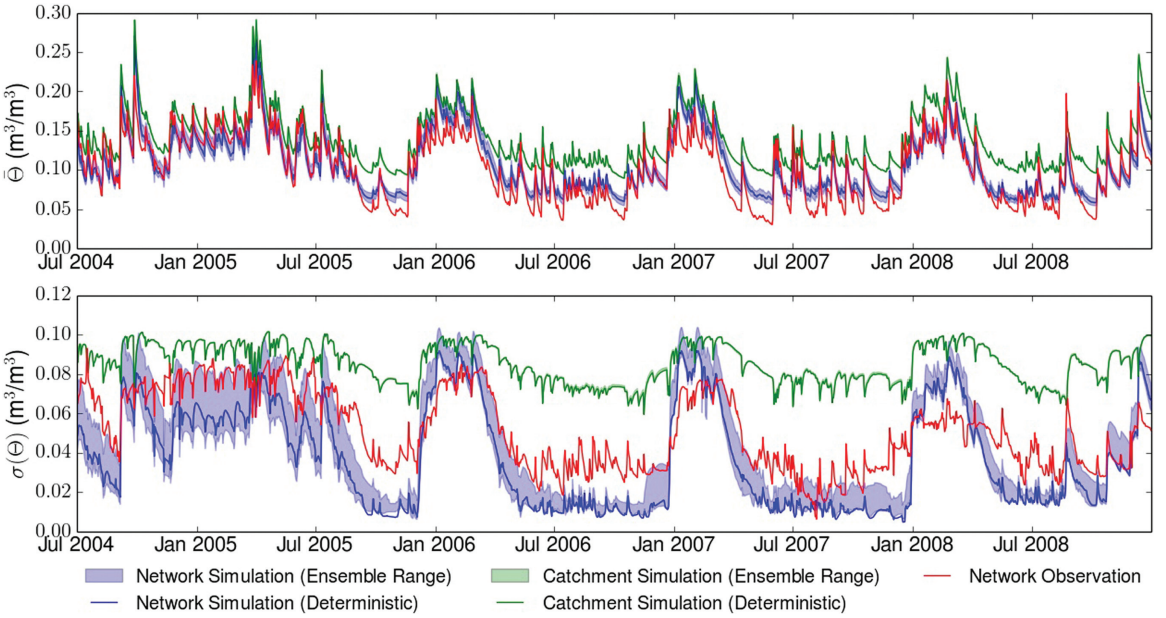


**Figure 13.** (top) The simulated and observed soil moisture mean and (bottom) standard deviation over the LREW between 2004 and 2008 using both the deterministic soil map and 10 soil ensembles (blue and green spread) from the SSURGO data set.

3-D histogram method consistently outperforms simple random sampling. The differences are more appreciable when trying to reproduce the time series of standard deviation; starting at 2 stations, the 3-D histogram networks consistently outperforms simple random sampling. When trying to capture spatial heterogeneity, the uncertainty bounds are also reduced when using the 3-D histogram sampling technique.

To understand the role of the drivers of soil moisture heterogeneity in the optimal 3-D histogram, Figure 12 shows the number of bins (for the proxy of each driver) used to build each network. Not surprisingly, up to 20 stations, all the binning goes to the soils-topographic index. After that it transitions to including soils and land cover. This could be because the binning cutoff is 20 or because it needs to sample the other drivers to increase performance.

## 5. Discussion

### 5.1. Input Data Uncertainty: Soil Properties

Soil heterogeneity is arguably the main source of input data uncertainty in this study; although SSURGO goes a long way in providing detailed spatial information, it still misses point scale heterogeneity that drives errors in capturing the soil moisture heterogeneity.

To assess the uncertainty of using only the representative values for each map-unit most frequent soil component (used throughout this study), TOPLATS is run using a set of soil ensembles built from the SSURGO uncertainty information. Following the work of *Odgers et al.* [2015], it is assumed that the value of each soil property can be drawn from a triangular distribution where the lower, upper, and representative values define the distribution. For each grid cell, each of the properties of all components in the map unit is sampled at random from its corresponding triangular distribution. A set of pedotransfer functions [*Maidment*, 1993] are then used to estimate missing parameters (e.g., residual soil moisture). The weighted average of the components is then computed for each 1/3 arc sec grid cell. For each of the 10 different ensembles of soil maps, TOPLATS is run using the SSMR technique at a 5 arc sec spatial resolution and the optimal parameter set found in section 4.1.1.

Figure 13 compares the ensemble spread of simulated soil moisture mean and standard deviation (catchment and network) to the observations and deterministic soil simulations. For small sample sizes (i.e., simulated network) the ensemble of soil properties makes a significant difference in the standard deviation.

There is an overall increase in soil moisture heterogeneity as compared to the deterministic simulation leading to at times bounding the observed heterogeneity during the dry periods. The network mean ensemble spread suggests the deterministic simulation captures the ensemble mean. For the catchment estimates, the simulated network results hold except that the ensemble spread is significantly reduced (practically negligible for both the mean and standard deviation).

The reduced ensemble spread of the catchment mean and standard deviation could be due to polygon heterogeneity playing a more dominant role than fine-scale soil heterogeneity, using a triangular distribution to model uncertainty, or errors in the SSURGO uncertainty estimates. Future work should look into more appropriate ways to capture the SSURGO uncertainty data and assess the impact of using other distributions to model uncertainty. The errors in the pedotransfer functions should also be included to comprehensively account for the drivers of uncertainty of soil hydraulic properties. This could lead to a better representation of fine-scale heterogeneity and help bound calibration procedures.

### 5.2. Hydrologic Similarity, Model Uncertainty, and Parameter Estimation

The hydrologic model (TOPLATS) is also a source of error. Although simulating hydrologic processes at 1/3 arc sec ($\sim$ 9 m) is close to the spatial scale of soil moisture probes, it is most likely still too coarse. One possibility would be to use the 3 m USGS NED product (currently in development) over CONUS to increase the DEM resolution. However, at that scale there will be an increasing discrepancy between the assumed (slope) and actual hydraulic gradient.

TOPMODEL's assumptions of an exponential transmissivity profile, uniform recharge rate, and constant upslope effective contributing area should also be addressed in TOPLATS. One possibility is to substitute the hydrologic model for Dynamic TOPMODEL that maintains the HSU concept while allowing dynamic subsurface redistribution [*Beven and Freer*, 2001]. The multiple layers and bedrock depth available through SSURGO could also provide information to construct the transmissivity profile and define the maximum depth. This work could also explore accounting for lateral flows in the unsaturated layer and accounting for the effects of reinfiltration and surface ponding on soil moisture heterogeneity.

### 5.3. Controls on the Spatial Variability of Soil Moisture

The analysis over the Little River Experimental Watershed suggests complex interactions between the main drivers of soil moisture heterogeneity (topography, soil properties, vegetation, and precipitation). The controlled simulations (section 4.2.1) show how soil heterogeneity increases soil moisture heterogeneity uniformly over time with limited interseasonal variations. Since the soils in the LREW are mainly loamy and sandy soils, this result is not surprising. Future work should consider the connection of the seasonality of soil moisture heterogeneity and more heterogeneous soils (e.g., a mix of sand and clay).

The influence of topography and vegetation on the soil moisture heterogeneity is correlated to the water table depth and plant phenology, respectively. In the winter, evapotranspiration is low and the water table is close to the surface leading to groundwater and subsurface flow playing a dominant control on heterogeneity. This is not as predominant during the summer, when the model water table tends to be deeper (less control on surface soil moisture patterns) and vegetation is more active and plays a more important role in soil moisture heterogeneity. This result coincides with previous studies that suggest the role of each driver of heterogeneity varies over time [*Rosenbaum et al*., 2012; *Western et al*., 1998].

Even after including all the drivers of heterogeneity, the model still fails to capture the observed spatial heterogeneity of soil moisture during the dry periods. This is probably due to the lack of topographic controls in the simulated network during this time (see Figure 7). During the dry periods, the network heterogeneity is likely controlled by soil and land cover heterogeneity that is not fully accounted for in the simulations due to their coarser effective spatial resolutions. Since previous work has shown that topography is rarely the single driver of soil moisture heterogeneity [e.g., *Wilson et al*., 2005], it is probable that the role of subsurface flow is exaggerated in the soils-topographic index (see Figure 3) and overcompensates for missing soil and land cover heterogeneity.

### 5.4. Network Design

The comparison of the simulated catchment mean and standard deviation to the actual and simulated networks suggest that the current network underestimates both measures especially during the

summer. During the winter, when the model water table is closer to the surface, transition areas in the catchment are close to saturation (see Figure 7) and act as proxies of the semipermanent saturated areas (floodplains and streambeds) in the current measurement network. During the drier periods (summer) these transition areas are drier and are not representative of the saturated regions leading to under sampling of moist regions in the catchment and an underestimation of the catchment's mean and standard deviation.

The proposed network design method (3-D histogram) improves the sampling of the catchment's characteristic regions by placing soil moisture probes in hydrologic similar units. However, placing soil moisture probes within regions with semipermanent standing water is not feasible; this could be replaced with a simple accounting for the total area of the catchment with permanent to semipermanent standing water. This would lead to improved estimates of the catchment mean and standard deviation from in situ networks that would in turn improve validation of satellite remote sensing of soil moisture.

It is acknowledged that the reliability of the proposed network design method is conditioned by the performance of the calibrated TOPLATS model (e.g., role of the soils-topographic index). To corroborate the results and test whether the current network underestimates the mean spatial heterogeneity, we propose testing the method over the Little River Experimental Watershed. This could be done by enhancing the current network with probes in missing areas suggested by the 3-D histogram.

### 5.5. Spatial Downscaling

Given the coarse spatial resolution of satellite retrievals of soil moisture, there is a recurring need for spatial downscaling techniques. One method is to simulate high-resolution soil moisture fields in parallel to the retrievals and simply scale each field using the corresponding retrieval. However, over regions where a high-resolution modeling framework is not feasible, there is a need for robust, simple, and transferable spatial downscaling techniques.

In regions where topography and soils play a dominant role in the soil moisture heterogeneity, the soils-topographic index could be used as a proxy of soil moisture patterns. As shown in Figure 7, the relationship between the soils-topographic index and the fine-scale volumetric water content over the LREW varies as a function of the catchment soil moisture mean. Assuming a functional relationship can be used to characterize this "flat-to-linear-to-flat" relationship at each time step (e.g., scaled error function), the parameters of the chosen function could then be related to the catchment mean. The technique could also account for soil heterogeneity by using the normalized soil water content instead of the volumetric water content.

## 6. Conclusions

The TOPLATS land surface model has been run over the Little River Experimental Watershed to produce high-resolution ($\sim$9 m) daily soil moisture fields between 2004 and 2008. Validation of the simulations using the observation network suggests the representation of subsurface redistribution in the model explains the skillful (yet biased) simulation of the seasonality of the soil moisture spatial heterogeneity. The role of the other drivers of soil moisture spatial heterogeneity (especially soils) is most likely underestimated and cannot be disregarded. The comparison of the full catchment simulations to the existing observation network suggests the current network fails to capture regions of persistent saturation in the catchment leading to an underestimation of the catchment mean and standard deviation.

To inform improved network design, a method is developed that takes advantage of hydrologic similarity to construct measurement networks that maximizes the coverage of catchment heterogeneity while minimizing the sample size. It is acknowledged that the novel method's skill can be connected to the model being used and should be tested by enhancing the network over the Little River Experimental Watershed. Hydrologic similarity was also used to explore a method for improved calibration and scalability of TOPLATS catchment parameters. Future work will use these concepts to extend the land cover tiling scheme in macroscale land surface models to topography and soil properties to provide an improved link between catchment and continental scale hydrologic modeling.

**Acknowledgments**
This study was supported by funding from NOAA grant NA08OAR4320915 (Ensemble Hydrologic Forecasts over the Southeast in Support of the NIDIS Pilot), NOAA grant NA11OAR4310175 (Improving land evaporative processes and land-atmosphere interactions in the NCEP Global Forecast System (GFS) and Climate Forecast System (CFS), and NSF grant 1144217 (Petascale Design and Management of Satellite Assets to Advance Space Based Earth Science). The data sets used in this study were obtained from the USDA NRCS, USDA-ARS, NCEP, NASA, and Beijing Normal University.

## References

Beven, K. J., and J. Freer (2001), A dynamic TOPMODEL, *Hydrol. Processes*, *15*, 1993–2001.
Beven, K. J., and M. J. Kirby (1979), A physically based, variable contributing area model of basin hydrology, *Hydrol. Sci.*, *24*, 43–69.
Bircher, S., N. Skou, K. H. Jensen, J. P. Walker, and L. Rasmussen (2012), A soil moisture and temperature network for SMOS validation in Western Denmark, *Hydrol. Earth Syst. Sci.*, *16*, 1445–1463.
Blöschl, G., and M. Sivapalan (1995), Scale issues in hydrological modelling: A Review, *Hydrol. Processes*, *9*, 251–290.
Bosch, D. D., J. M. Sheridan, R. R. Lowrance, R. K. Hubbard, T. C. Strickland, G. W. Feyereisen, and D. G. Sullivan (2007), Little River Experimental Watershed Database, *Water Resour. Res.*, *43*, W09470, doi:10.1029/2006WR005844.
Chaney, N. W., J. Sheffield, G. Villarini, and E. F. Wood (2014), Development of a high-resolution gridded daily meteorological dataset over sub-saharan Africa: Spatial analysis of trends in climate extremes, *J. Clim.*, *27*(15), 5815–5835.
Ciach, G. J., and W. F. Krajewski (2006), Analysis and modeling of spatial correlation structure in small-scale rainfall in Central Oklahoma, *Adv. Water Resour.*, *29*, 1450–1463.
Crow, W. T., D. Ryu, and J. S. Famiglietti (2005), Upscaling of field-scale soil moisture measurements using distributed land surface modeling, *Adv. Water Resour.*, *28*, 1–14.
Crow, W. T., A. A. Berg, M. H. Cosh, A. Loew, B. P. Mohanty, R. Panciera, P. de Rosnay, D. Ryu, and J. P. Walker (2012), Upscaling sparse ground-based soil moisture observations for the validation of coarse-resolution satellite soil moisture products, *Rev. Geophys.*, *50*, RG2002, doi:10.1029/2011RG000372.
Famiglietti, J. S., and E. F. Wood (1994), Multiscale modeling of spatially variable water and energy balance processes, *Water Resour. Res.*, *30*(11), 3061–3078.
Famiglietti, J. S., J. W. Rudnicki, and M. Rodell (1998), Variability in surface moisture content along a hillslope transect: Rattlesanke Hill, Texas, *J. Hydrol.*, *210*, 259–281.
Famiglietti, J. S., D. Ryu, A. A. Berg, M. Rodell, and T. J. Jackson (2008), Field observations of soil moisture variability across scales, *Water Resour. Res.*, *44*, W01423, doi:10.1029/2006WR005804.
Friesen, J., C. Rodgers, P. G. Oguntunde, J. M. H. Hendrickx, and N. van de Giesen (2008), Hydrotope-based protocol to determine average soil moisture over large areas for satellite calibration and validation with results from an observation campaing in the volta basin, West Africa, *IEEE Trans. Geosci. Remote Sens.*, *46*(7), 1995–2004.
Fry, J., G. Xian, S. Jin, J. Dewitz, C. Homer, L. Yang, C. Barnes, N. Herold, and J. Wickham (2011), Completion of the 2006 National Land Cover Database for the Conterminous United States, *Photogramm. Eng. Remote Sens.*, *77*(9), 858–864.
Gesch, D., G. Evans, J. Mauck, J. Hutchinson, and W. J. Carswell Jr. (2009), The National Map-Elevation, *U.S. Geol. Surv. Fact Sheet, 2009–3053*, 4 pp.
Grayson, R. B., A. W. Western, F. Chiew, H. S., and G. Blöschl (1997), Prefered states in spatial soil moisture patterns: Local and nonlocal controls, *Water Resour. Res.*, *33*(12), 2897–2908.
Gupta, V. H., H. Kling, K. K. Yilmaz, and G. F. Martinez (2009), Decomposition of the mean squared error and NSE performance criteria: Implications for improving hydrological modelling, *J. Hydrol.*, *377*(1–2), 80–91.
Hawley, M. E., T. J. Jackson, and R. H. McCuen (1983), Surface soil moisture variation on small agricultural watersheds, *J. Hydrol.*, *62*, 179–200.
Jackson, T. J., M. H. Cosh, X. Zhang, D. D. Bosch, D. D. Seyfried, P. J. Starks, T. Keefer, and V. Lakshmi (2006), Validation of AMSR-E soil moisture products using watershed networks, paper presented at the International Geoscience and Remote Sensing Symposium, IEEE Geosci. and Remote Sens. Soc., Denver, Colo., 31 Jul to 4 Aug.
Lin, Y., and K. E. Mitchell (2005), The NCEP stage II/IV hourly precipitation analyses: Development and applications, paper presented at 19th Conference on Hydrology, Am. Meteorol. Soc., San Diego, Calif., 9–13 Jan.
Maidment, D. R. (1993), *Handbook of Hydrology*, McGraw-Hill, N. Y.
McKay, M. D., R. J. Beckman, and W. J. Conover (1979), A comparison of three methods for selecting values of input variables in the analysis of output from a computer code, *Technometrics*, *21*(2), 239–245.
Mohanty, B. P., J. S. Famiglietti, and T. H. Skaggs (2000), Evolution of soil moisture spatial structure in a mixed vegetation pixel during the Southern Great Plains 1997 (SGP97) hydrology experiment, *Water Resour. Res.*, *36*(12), 3675–3686, doi:10.1029/2000WR900258.
Meals, D. W., et al. (2012), Little River Experimental Watershed, Georgia: National Institute of Food and Agriculture-Conservation Effects Assessment Project, in *How to Build Better Agricultural Conservation Programs to Protect Water Quality: The National Institute of Food and Agriculture-Conservation Effects Assessment Project Experience*, edited by D. L. Osmond, et al., pp. 187–200, Soil and Water Conserv. Soc., Ankeny, Iowa.
Odgers, N. P., A. B. McBratney, and B. Minasny (2015), Digital soil property mapping and uncertainty estimation using soil class probability rasters, *Geoderma*, *237–238*, 190–198.
Page, T., K. J. Beven, J. Freer, and C. Neal (2007), Modelling the chloride signal at Plynlimon, Wales, using a modified dynamic TOPMODEL incorporating conservative chemical mixing (with uncertainty), *Hydrol. Processes*, *21*, 292–307.
Pan, F., and C. D. Peters-Lidard (2008), On the relationship between mean and variance of soil moisture fields, *J. Am. Water Resour. Assoc.*, *44*(1), 235–242.
Pauwels, V. R. N., and E. F. Wood (1999), A soil-vegetation-atmosphere transfer scheme for the modeling of water and energy balance processes in high latitudes. 1: Model improvements, *J. Geophys. Res.*, *104*(D22), 27,811–27,822.
Peters-Lidard, C. D., M. S. Zion, and E. F. Wood (1997), A soil-vegetation-atmosphere transfer scheme for modeling spatially variable water and energy balance processes, *J. Geophys. Res.*, *102*(D4), 4303–4324.
Quinn, P., K. Beven, and A. Culf (1995), The introduction of macroscale hydrological complexity into land-surface transfer models and the effect on planetary boundary layer development, *J. Hydrol.*, *166*, 421–444.
Rodriguez-Iturbe, I., and A. Porporato (2004), *Ecohydrology of Water-Controlled Ecosystems: Soil Moisture and Plant Dynamics*, 442 pp., Cambridge Univ. Press, N. Y.
Rosenbaum, U., H. R. Bogena, M. Herbst, J. A. Huisman, T. J. Peterson, A. Weuthen, A. W. Western, and H. Vereecken (2012), Seasonal and event dynamics of spatial moisture patterns at the small catchment scale, *Water Resour. Res.*, *48*, W10544, doi:10.1029/2011WR011518.
Schwanghart, W., and N. J. Kuhn (2010), TopoToolbox: A set of Matlab functions for topographic analysis, *Environ. Modell. Software*, *25*, 770–781.
Shirmohammadi, A., J. M. Sheridan, and L. E. Asmussen (1986), Hydrology of alluvial stream channels in southern Coastal Plain watersheds, *Trans. ASAE*, *29*, 135–142.
Sivapalan, M., K. Beven, and E. F. Wood (1987), On hydrologic similarity. 2: A scaled model of storm runoff production, *Water Resour. Res.*, *23*(12), 2266–2278.

Soil Survey Staff (2012), Natural Resources Conservation Service, United States Department of Agriculture, Soil Survey Geographic (SSURGO) Database. [Available at http://sdmdataaccess.nrcs.usda.gov/, last accessed 10 Aug 2012.]

Tarboton, D. G. (1997), A new method for the determination of flow directions and contributing areas in grid digital elevation models, *Water Resour. Res.*, *33*(2), 309–319.

Vereecken, H., T. Kamai, T. Harter, R. Kastell, J. Hopmans, and J. Vanderborght (2007), Explaining soil moisture variability as a function of mean soil moisture: A stochastic unsaturated flow perspective, *Geophys. Res. Lett.*, *34*, L22402, doi:10.1029/2007GL031813.

Villarini, G., P. V. Mandapaka, W. F. Krajewski, and R. J. Moore (2008), Rainfall and sampling uncertainties: A rain gauge perspective, *J. Geophys. Res.*, *113*, D11102, doi:10.1029/2007JD009214.

Vivoni, E. R., J. C. Rodriguez, and C. J. Watts (2010), On the spatiotemporal variability of soil moisture and evapotranspiration in a mountainous basin within the North American monsoon region, *Water Resour. Res.*, *46*, W02509, doi:10.1029/2009WR008240.

Western, A. W., G. Blöschl, and R. B. Grayson (1998), Geostatistical characterisation of soil moisture patterns in the Tarrawarra catchment, *J. Hydrol.*, *205*, 20–37.

Western, A. W., R. B. Grayson, G. Blöschl, G. R. Willgoose, and T. A. McMahon (1999), Observed spatial organization of soil moisture and its relation to terrain indices, *Water Resour. Res.*, *35*(3), 797–810.

Western, A. W., S. Zhou, R. B. Grayson, T. A. McMahon, G. Blöschl, and D. J. Wilson (2004), Spatial correlation of soil moisture in small catchments and its relationship to dominant spatial hydrological processes, *J. Hydrol.*, *286*, 113–134.

Wilson, D. J., A. W. Western, and R. B. Grayson (2005), A terrain and data-based method for generating the spatial distribution of soil moisture, *Adv. Water Resour.*, *28*, 43–54.

Xia, Y., et al. (2012), Continental-scale water and energy flux analysis and validation for the North American Land Data Assimilation System project phase 2 (NLDAS-2). 1: Intercomparison and application of model products, *J. Geophys. Res.*, *117*, D03109, doi:10.1029/2011JD016048.

Yuan, H., Y. Dai, Z. Xiao, J. D., and W. Shangguan (2011), Reprocessing the MODIS leaf area index products for land surface and climate modelling, *Remote Sens. Environ.*, *115*(5), 1171–1187.